Linear Parameter Varying Pitch Autopilot Design for a class of Long Range Guided Projectiles

Gian Marco Vinco, Spilios Theodoulis, Olivier Sename, Guillaume Strub

HAL Id: hal-04036268

https://hal.univ-grenoble-alpes.fr/hal-04036268

Submitted on 19 Mar 2023

Linear Parameter Varying Pitch Autopilot Design for a class of Long Range Guided Projectiles

Gian Marco VINCO*

University Grenoble Alpes, CNRS, Grenoble INP, GIPSA-Lab, 38000,Grenoble, France and French-German Research Institute of Saint-Louis, Saint-Louis, 68300, France

Spilios THEODOULIS†

Delft University of Technology, Faculty of Aerospace Engineering, 2629, Delft, The Netherlands

Olivier SENAME‡

University Grenoble Alpes, CNRS, Grenoble INP, GIPSA-Lab, 38000,Grenoble, France

Guillaume STRUB§

French-German Research Institute of Saint-Louis, Saint-Louis, 68300, France

Promising results on LPV design have been recently proposed, concerning the modeling and control of missiles, rockets, and aircraft. However, very few investigations have been focused on the development of guided projectile applications. This paper presents a pure linear parameter varying (LPV) modeling and control design approach intended to improve the range capability of a new class of Long Range Guided Projectiles (LRGP). The investigated concept consists of an asymmetric 155 mm fin-stabilized projectile equipped with a reduced amount of control actuators and characterized by a predominant unstable behavior across the analyzed flight envelope. The main advantages of the LPV design in terms of guaranteed robustness and stability are compared to standard gain-scheduling-based linear time-invariant (LTI) control strategies. A nonlinear simulation scenario is performed in order to assess the reliability of a pure LPV autopilot design, based on the polytopic formulation, across the entire flight envelope, over a local modal control design related to a specific set of flight conditions.

I. Introduction

In the last decades, the Linear Parameter Varying (LPV) framework has attracted increasing interest in the modeling and the control of a wide range of aerospace applications. Initial studies presented the LPV modeling approach as a perfect match for the well-established gain-scheduling controller design technique, leading to relevant contributions both in terms of missile [1–5], and aircraft [6–8] applications. Important studies have also focused on the investigation of guided projectiles, intending to improve the accuracy and the range capability of artillery operations. LPV modeling of projectiles has been coupled with the employment of robust control design for both spin-stabilized [9–11] and fin-stabilized [12, 13] architectures. However, the LPV models were generally obtained as a collection of local linearizations of the original nonlinear dynamics unable to fully characterize the dynamics of the system, with the possible loss of important information regarding the transient behavior. The gain-scheduled autopilots result from the interpolation of the corresponding set of linear time-invariant (LTI) controllers, designed at the trimming conditions selected during the model linearization. Consequently, important properties such as stability and flight performances are only guaranteed around the analyzed trimming points, but not at all the remaining flight conditions [14, 15].

These limitations motivated the investigation of alternative LPV-based design approaches, providing a better representation of the full system dynamics [16–18], as well as robustness and performance properties across the entire flight envelope [19–22]. Concerning guided projectiles, only recently, an LPV approach has been developed [23], in the

---

*Ph.D. Student, GIPSA-lab, 11 rue des Mathématiques, 38402, Saint Martin d'Hères, France, Gian-Marco.Vinco@grenoble-inp.fr.

†The author was with the French-German Research Institute of Saint-Louis, 68300, Saint-Louis, France. He is now an Associate Professor at the Delft University of Technology, Control & Operations Department, Room LB 0.23, Kluyverweg 1, 2629 HS Delft, The Netherlands, Spilios.Theodoulis@isl.eu, AIAA Senior Member.

‡Professor, GIPSA-lab, 11 rue des Mathématiques, 38402, Saint Martin d'Hères, France, Olivier.Sename@grenoble-inp.fr.

§Researcher Scientist, Guidance Navigation & Control Department, 5 rue du Général Cassagnou, 68300, Saint-Louis, France, Guillaume.Strub@isl.eu.

framework of Model Predictive Control (MPC), opening several opportunities to be further investigated. This paper intends to propose a pure LPV H_∞ controller design for the pitch channel dynamics of a new class of *Long Range Guided Projectiles* (LRGP), aiming to improve the operating range of artillery operations employing a Bank-To-Turn gliding flight strategy. Interesting properties of the analyzed concept derive from the selection of a reduced set of control actuators, leading to an asymmetric canards/fins configuration [24, 25], and a predominant statically unstable behavior. Recent research on long-range guided projectiles [26] underlined the impact of the canards/fins configuration, aerodynamics modeling, and guidance development on the overall range capability. In a previous study, the full nonlinear dynamics of the projectile have been derived [27], and converted into a corresponding quasi-LPV model through the State Transformation technique [28], trying to minimize the need for model approximations.

The LPV autopilot design discussed here relies on a polytopic formulation. First introduced in [29], the polytopic approach allows the formulation of the synthesis of a controller that guarantees stability and performance for any conditions of the varying parameters in a selected subset, by only targeting the extreme values characterizing each parameter in that subset. However, the polytopic formulation implies the definition of a convex space of parameter variations and requires an affine model-parameters relation. As a consequence, the optimization process can be affected by an excessive level of conservatism that can deteriorate performance of the controller. These aspects are extensively investigated in the present work, where a modeling procedure is proposed to generate a quasi-LPV model for the projectile that complies with the requirements of the polytopic formulation and reduces the conservativeness. The obtained control results are coupled in simulations with a preliminary ad-hoc implemented guidance law, targeting the optimization of the aerodynamic angle-of-attack during the gliding phase of the trajectory [30, 31].

The proposed article is divided as follows. The pitch channel nonlinear dynamics of the guided projectile is first discussed in Section II, as well as the derivation of the corresponding quasi-LPV model. In Section III, the theoretical formulation of the LPV polytopic class of systems is presented. A complete approximation analysis allows reformulating the obtained quasi-LPV model to satisfy the polytopic requirements. Once the accuracy of the approximations is verified, the dimensions of the investigated flight envelope are optimized to reduce the complexity of the controller synthesis process. Later, Section IV details the generalized scheme employed for the robust controller synthesis. A design comparison between the frequency performance of an LPV H_∞ polytopic controller and a modal state feedback controller, based on the pole placement approach, assesses the advantages of the LPV formulation over a standard LTI control design. Finally, in Section V, a reference tracking simulation scenario is proposed, employing the LPV polytopic controller to target an angle-of-attack guidance trajectory. The ultimate purpose is to prove the capability of the LPV design, to ensure competitive performances and stability properties across all the conditions described by the selected flight envelope, which are not guaranteed a priori by standard LTI gain-scheduled controllers.

II. Projectile Pitch Channel Dynamics

This section provides a description of the projectile physical concept, design properties, and operational objectives. The full nonlinear model related to the pitch channel dynamics is described, including some relevant insights concerning the aerodynamic characterization and the control input allocation. Later, the nonlinear model is converted into a corresponding quasi-LPV one using the State Transformation technique. The obtained quasi-LPV model will be formulated as a polytopic system in the next section and employed for the different controller designs, while the performances of the resulting autopilot are intended to be tested directly on the nonlinear dynamic model.
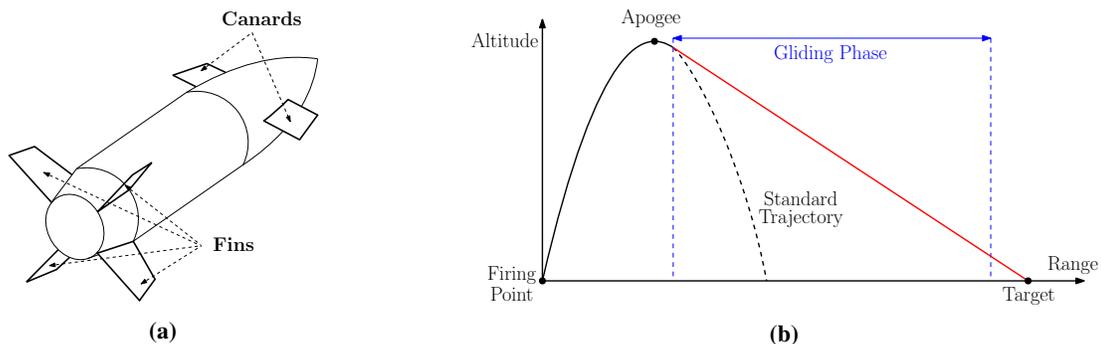

Fig. 1   Long Range Guided Projectile: (a) projectile concept; (b) range enhancement flight strategy.

A. Nonlinear Model

The investigated nonlinear model refers to a 155 mm fin-stabilized guided projectile, characterized by a set of two front control canards, and a set of four symmetrical rear fins, non-co-planar to the plane of symmetry of the canards, as shown in Fig. 1(a). The reduced amount of control surfaces, that affects the resulting control authority, is justified by the intention of improving the projectile operating range through a Bank-To-Turn (BTT) flight strategy employed during the gliding phase of the trajectory, as is shown in Fig. 1(b).

The full nonlinear model of the projectile, including the analysis and derivation of the aerodynamic contributions, was discussed in a previous work [27]. For the purposes of this study, we focus the analysis on the pitch channel of the projectile only, consisting of the dynamics of the aerodynamic angle-of-attack, α, and of the pitch rate, q, expressed with respect to the system of coordinates integral to the projectile body:

$$
\begin{aligned}
\dot{\alpha} &= -\frac{X \sin \alpha}{mV \cos \beta} + \frac{Z \cos \alpha}{mV \cos \beta} + \frac{g}{V \cos \beta} \left(\sin \alpha \sin \theta + \cos \alpha \cos \theta \cos \phi \right) + q - p \tan \beta \cos \alpha - r \tan \beta \sin \alpha, \\
\dot{q} &= \frac{1}{I_{yy}} \left[M - pr \left(I_{xx} - I_{zz} \right) \right].
\end{aligned}
\tag{1}
$$

The lateral contributions of the yaw rate and the aerodynamic sideslip-angle, r and β, respectively, as well as the influence of the roll angle and the roll rate, ϕ and p, respectively, are assumed to be negligible for the pitch channel dynamics. Indeed, the sideslip-angle minimization (BTT) strategy, together with the particular geometry of the concept, allows the decoupling of the projectile dynamics between its lateral and pitch axes. The variation of the pitch angle, θ, is not accounted as a parameter to be included in the LPV analysis, so a nominal value was selected based on a set of simulation tests. The term V represents the true airspeed in zero relative wind conditions.

In terms of physical parameters, I_{xx}, I_{yy}, and I_{zz} correspond to the moments of inertia relative to the principal axes of the projectile body, m stands for the overall mass, and g for the standard acceleration of gravity, under flat Earth assumptions. Due to the characteristic second-order rotational symmetry of the projectile body, the off-diagonal inertia couplings terms, I_{xy}, I_{yz}, and I_{xz}, present in the inertia matrix, are neglected as well.

Additionally, the pitch channel dynamics is highly affected by the aerodynamics contributions, in the form of longitudinal and vertical forces, X and Z, and pitching moment, M, modeled through an extensive regression analysis based on a set of Computational Fluid Dynamics (CFD) data, as follows:

$$
\begin{aligned}
X &= \bar{q}S \left(C_{X_{\alpha 0}} + C_{X_{\alpha 2}} \sin^2 \alpha + C_{X_{\alpha 4}} \sin^4 \alpha + C_{X_{\delta_0}} + C_{X_{\delta_2}} \sin^2 \delta_{\text{eff}} \right), \\
Z &= \bar{q}S \left[C_{Z_{\alpha 1}} \sin \alpha + \left(\frac{d}{V} \right) C_{Z_{\mathrm{D}}} q + C_{Z_{\delta_1}} \sin \delta_q + C_{Z_{\delta_3}} \sin^3 \delta_q \right], \\
M &= \bar{q}Sd \left[C_{m_{\alpha 1}} \sin \alpha + C_{m_{\alpha 3}} \sin^3 \alpha + C_{m_{\alpha 5}} \sin^5 \alpha + \left(\frac{d}{V} \right) C_{m_{\mathrm{D}}} q + C_{m_{\delta_1}} \sin \delta_q + C_{m_{\delta_3}} \sin^3 \delta_q \right].
\end{aligned}
\tag{2}
$$

The aerodynamic model is defined by the values of the reference surface S and caliber d, the dynamic pressure $\bar{q} = \frac{1}{2} \rho \left(h \right) V^2$, function of the altitude h and the air density ρ, and by the set of aerodynamics regression coefficients related to the longitudinal static ($C_{X_{\alpha 0}}$, $C_{X_{\alpha 2}}$, $C_{X_{\alpha 4}}$) and control ($C_{X_{\delta_0}}$, $C_{X_{\delta_2}}$) forces, to the vertical static ($C_{Z_{\alpha 1}}$), dynamic ($C_{Z_{\mathrm{D}}}$), and control ($C_{Z_{\delta_1}}$, $C_{Z_{\delta_3}}$) forces, and finally to the pitching static ($C_{m_{\alpha 1}}$, $C_{m_{\alpha 3}}$, $C_{m_{\alpha 5}}$), dynamic ($C_{m_{\mathrm{D}}}$), and control ($C_{m_{\delta_1}}$, $C_{m_{\delta_3}}$) moments. Each of the previous aerodynamic coefficients has been obtained as a function of a selected range of subsonic Mach values, $\mathcal{M}$.

Furthermore, the local deflection angles characterizing the right and the left control canards, δ_{r} and δ_{l}, respectively, are allocated into a set of virtual deflections. The virtual set expresses the control action in terms of a roll contribution, δ_p, and a pitch contribution, δ_q, obtained respectively through a differential or a concurrent deflection of the individual surfaces, following the allocation strategy:

$$
\begin{bmatrix} \delta_p \\ \delta_q \end{bmatrix} = \begin{bmatrix} -\frac{1}{2} & +\frac{1}{2} \\ +\frac{1}{2} & +\frac{1}{2} \end{bmatrix} \begin{bmatrix} \delta_{\text{r}} \\ \delta_{\text{l}} \end{bmatrix}.
\tag{3}
$$

The longitudinal control contribution, δ_{eff}, was modeled as a nonlinear combination of the virtual roll and pitch deflections and represents a braking effect due to the additional drag generated by canards deflections.

B. Quasi-LPV Model

The nonlinear dynamics in Eqs. (1)-(3), can be reformulated in a more compact fashion, as an output nonlinear system. However, this formulation requires the system to be affine in the input, thus a first-order approximation of the aerodynamic control coefficients ($C_{Z_{\delta_1}}$, $C_{Z_{\delta_3}}$, $C_{m_{\delta_1}}$, $C_{m_{\delta_3}}$) was investigated in detail in [28], and applied to the pitch channel dynamics. The resulting nonlinear *Simplified* model is used for the LPV modeling and control design, assuming the aerodynamic approximations as a source of uncertainties to be handled by the controller. The remaining nonlinear contributions characterizing the model are functions of the set of continuous time-varying parameters, $\rho(t)$, and can be collected in the generalized terms $f_1(\rho)$ and $f_2(\rho)$, as it follows:

$$\begin{bmatrix} \dot{\alpha} \\ \dot{q} \end{bmatrix} = \begin{bmatrix} f_1(\rho) \\ f_2(\rho) \end{bmatrix} + \begin{bmatrix} 0 & A_{12}(\rho) \\ 0 & A_{22}(\rho) \end{bmatrix} \begin{bmatrix} \alpha \\ q \end{bmatrix} + \begin{bmatrix} B_1(\rho) \\ B_2(\rho) \end{bmatrix} \delta_q; \qquad \rho(t) = [\alpha(t), V(t), h(t)] \tag{4}$$

where:

$$\begin{aligned}
A_{12}(\rho) &:= 1 + \frac{\bar{q}SdC_{Z_\mathrm{D}} \cos\alpha}{2mV^2}; & B_1(\rho) &:= \frac{\bar{q}SC_{Z_{\delta_1}} \cos\alpha}{mV}; \\
A_{22}(\rho) &:= \frac{\bar{q}Sd^2C_{m_\mathrm{D}}}{2I_{\mathrm{yy}}V}; & B_2(\rho) &:= \frac{\bar{q}SdC_{m_{\delta_1}}}{I_{\mathrm{yy}}}.
\end{aligned} \tag{5}$$

Starting from the nonlinear *Simplified* pitch channel dynamics in Eqs. (4)-(5), a reliable quasi-LPV model can be obtained by employing a systematic State Transformation technique [1, 2]. The complete derivation of the LPV model from the nonlinear *Simplified* one is detailed in [28]. Despite being restricted to a limited class of systems, the State Transformation approach provides a quasi-LPV model which corresponds to an exact transformation of the original nonlinear system, avoiding any form of additional approximations. In particular, the transformation aims to hide the nonlinear parameter-varying terms $f_1(\rho)$ and $f_2(\rho)$ present in the model through a redefinition of the non-scheduling state variables and of the input of the system, respectively q and δ_q in Eq. (4). The new state vector of the quasi-LPV pitch channel dynamics model includes the angle-of-attack, α, and the off-equilibrium values of the pitch rate, q_dev, and of the virtual pitch deflection, $\delta_{q,\mathrm{dev}}$, defined during the transformation process as:

$$q_\mathrm{dev} = q - q_\mathrm{eq}(\rho); \qquad \delta_{q,\mathrm{dev}} = \delta_q - \delta_{q,\mathrm{eq}}(\rho), \tag{6}$$

where the equilibrium function $q_\mathrm{eq}(\rho)$ and $\delta_{q,\mathrm{eq}}(\rho)$, are obtained by trimming the pitch channel dynamics of the projectile in Eqs. (4)-(5) across the entire flight envelope described by the variation of the scheduling vector $\rho(t)$. The dynamics of the off-equilibrium variables, $q_\mathrm{dev}(t)$ and $\delta_{q,\mathrm{dev}}(t)$, are expressed through the derivatives of the corresponding equilibrium functions, $q_\mathrm{eq}(\rho)$ and $\delta_{q,\mathrm{eq}}(\rho)$, respectively.

Finally, the inclusion of an integrator at the input of the system defines the new input $\sigma = \int \delta_q$. This solution allows to remove the dependence of the input from the current equilibrium flight configuration, which was introduced by the transformation process in $\delta_{q,\mathrm{dev}}(t)$ and can strongly affect the stability of the system [17]. Additionally, the integration redefines the input matrix, B, of the quasi-LPV system in a parameter-independent form expressed by the identity matrix, I, which is a fundamental requirement for the later LPV control design. From a modeling perspective, the presence of the integrator can be justified by assuming that the controller intended to be developed accounts for a pure integral action that is formally included in the system definition.

The resulting *Augmented* quasi-LPV model of the projectile pitch channel dynamics is expressed as:

$$\begin{bmatrix} \dot{\alpha} \\ \dot{q}_\mathrm{dev} \\ \dot{\delta}_{q,\mathrm{dev}} \end{bmatrix} = \begin{bmatrix} 0 & A_{12}(\rho) & B_1(\rho) \\ 0 & \tilde{A}_{22}(\rho) & \tilde{B}_2(\rho) \\ 0 & \tilde{A}_{32}(\rho) & \tilde{B}_3(\rho) \end{bmatrix} \begin{bmatrix} \alpha \\ q_\mathrm{dev} \\ \delta_{q,\mathrm{dev}} \end{bmatrix} + \begin{bmatrix} 0 \\ 0 \\ I \end{bmatrix} \sigma, \tag{7}$$

with:

$$\begin{aligned}
\tilde{A}_{22}(\rho) &:= A_{22}(\rho) - \frac{\partial q_\mathrm{eq}}{\partial\alpha} A_{12}(\rho); & \tilde{B}_2(\rho) &:= B_2(\rho) - \frac{\partial q_\mathrm{eq}}{\partial\alpha} B_1(\rho); \\
\tilde{A}_{32}(\rho) &:= -\frac{\partial \delta_{q,\mathrm{eq}}}{\partial\alpha} A_{12}(\rho); & \tilde{B}_3(\rho) &:= -\frac{\partial \delta_{q,\mathrm{eq}}}{\partial\alpha} B_1(\rho).
\end{aligned} \tag{8}$$

4

III. Polytopic Model

In this section, the *Augmented* quasi-LPV model of the projectile in Eqs. (7)-(8) is reformulated as a polytopic system, in view of the control design. The main theoretical features and requirements of the polytopic class of systems are first discussed to verify which aspects of the obtained quasi-LPV model have to be adjusted to comply with the polytopic formulation. Later, a full model-parameter dependence analysis is presented, aiming to accurately approximate the quasi-LPV model, by mapping the original set of scheduling variables into a new set of scheduling functions that respect the polytopic considerations. Finally, an investigation of the dimensions of the polytope defined by the new set of functions is proposed to minimize the conservatism and the computational complexity of the controller synthesis.

A. LPV Polytopic Background

The polytopic formulation proposed here is based on [29], complying with the same notation. As previously mentioned, this approach is restricted to a class of LPV systems characterized by an affine dependence on the selected set of time-varying scheduling variables $\rho(t) = [\rho_1, \ldots, \rho_N]$. Additionally, the system is expected to be input and output parameter-independent to satisfy the affine conditions. The latter restriction can be generally relaxed by pre-filtering the input and the output. Finally, measurements of scheduling variables are supposed to be available in real-time, while their variation is assumed to be bounded between a minimum and a maximum value:

$$\underline{\rho_j} \leq \rho_j \leq \overline{\rho_j}$$

where $j \in [1, n_\rho]$, and $\overline{\rho_j}$, $\underline{\rho_j}$ indicate the upper and lower bounds, respectively, of the jth scheduling variable. The overall set of possible combinations of the variables boundary values defines a convex subspace (polytope) of 2^{n_ρ} vertices $\omega = [\omega_1, \ldots, \omega_{2^{n_\rho}}]$, where at each vertex, $\omega_i = [v_{i1}, \ldots, v_{in_\rho}]$ with $i \in [1, 2^{n_\rho}]$, the jth scheduling variable, v_{ij}, equals either $\overline{\rho_j}$ or $\underline{\rho_j}$. The corresponding set of LTI realizations of the system evaluated at each vertex of the polytope allows to obtain a general representation of the LPV system as the convex interpolation:

$$\left[\begin{array}{c|c} A(\rho) & B(\rho) \\ \hline C(\rho) & D(\rho) \end{array} \right] = \sum_{i=1}^{2^{n_\rho}} \mu_i \left[\begin{array}{c|c} A(\omega_i) & B(\omega_i) \\ \hline C(\omega_i) & D(\omega_i) \end{array} \right]. \tag{9}$$

In the specific case related to the model in Eqs. (7)-(8), the input matrix $B \in \mathbb{R}^{3x1}$ and the output matrix $C \in \mathbb{R}^{3x3}$ are constant parameter-independent, while the matrix $D = 0$. Additionally, from the scheduling vector in Eq. (4), $n_\rho = 3$.

The interpolation function $\mu_i(\rho)$ is computed for each vertex as follows:

$$\mu_i(\rho) = \frac{\displaystyle\prod_{j=1}^{n_\rho} |\rho_j - C^c(\omega_i)_j|}{\displaystyle\prod_{j=1}^{n_\rho} (\overline{\rho_j} - \underline{\rho_j})} > 0; \qquad \sum_{i=1}^{2^{n_\rho}} \mu_i(\rho) = 1, \tag{10}$$

where $C^c(\omega_i)_j$ indicates the jth element of the vector $C^c(\omega_i)$, as follows:

$$C^c(\omega_i)_j = \begin{cases} \overline{\rho_j} & if \ \omega_i = \underline{\rho_j} \\ \underline{\rho_j} & otherwise \end{cases}$$

B. Polytopic Modeling Process

Despite the input-parameter dependence being corrected by the inclusion of the integrator, the *Augmented* quasi-LPV model in Eqs. (7)-(8) is non-affine with respect to the selected set of scheduling variables, $\rho(t) = [\alpha(t), V(t), h(t)]$. Thus, it can not be directly reformulated as a polytopic system. In particular, the derivatives of the equilibrium functions, $q_{\text{eq}}(\rho)$ and $\delta_{q,\text{eq}}(\rho)$, included respectively in $\tilde{A}_{22}(\rho)$, $\tilde{B}_2(\rho)$ and $\tilde{A}_{32}(\rho)$, $\tilde{B}_3(\rho)$, correspond to complex nonlinear functions of all the three scheduling variables. A possible solution consists of mapping $\rho(t)$ into a new set of scheduling functions, $\tilde{\rho}(t)$, which satisfies the affine restriction imposed by the polytopic formulation. In the following, a full parameter dependence analysis is performed on the quasi-LPV system, trying to derive a new set $\tilde{\rho}(t)$ characterized by a number of scheduling functions lower or equal to the original one, $n_{\tilde{\rho}} \leq n_\rho = 3$. Indeed, the computational complexity related to the later controller synthesis tends to rapidly increase with the number of scheduling variables as $O(2^{n_\rho})$.

In the analysis, all the nonlinear terms characterizing the state matrix in Eq. (7) are considered and accounted for as possible functions of the new set $\tilde{\rho}(t)$. The process of approximation allows reducing step by step the resulting $n_{\tilde{\rho}}$ down to a feasible number. The full set of analyzed scheduling functions includes:

$$\tilde{\rho}_1 := \frac{\bar{q}SdC_{Z_D}\cos\alpha}{2mV^2}; \qquad \tilde{\rho}_2 := \frac{\bar{q}SC_{Z_{\delta_1}}\cos\alpha}{mV}; \qquad \tilde{\rho}_3 := \frac{\partial q_{\text{eq}}}{\partial\alpha};$$

$$\tilde{\rho}_4 := \frac{\partial\delta_{q,\text{eq}}}{\partial\alpha}; \qquad \tilde{\rho}_5 := \frac{\bar{q}Sd^2C_{m_D}}{2I_{yy}V}; \qquad \tilde{\rho}_6 := \frac{\bar{q}SdC_{m_{\delta_1}}}{I_{yy}}. \qquad (11)$$

As a consequence, the state matrix A can be reformulated as a function of the new set, $\tilde{\rho}(t)$, as:

$$A(\tilde{\rho}) = \begin{bmatrix} 0 & (1+\tilde{\rho}_1) & \tilde{\rho}_2 \\ 0 & \tilde{\rho}_5 - \tilde{\rho}_3(1+\tilde{\rho}_1) & \tilde{\rho}_6 - \tilde{\rho}_3\tilde{\rho}_2 \\ 0 & -\tilde{\rho}_4(1+\tilde{\rho}_1) & -\tilde{\rho}_4\tilde{\rho}_2 \end{bmatrix}. \qquad (12)$$

The analysis consists of the evaluation of the variation of each $\tilde{\rho}(t)$ entry, as a function of the original flight envelope defined by the scheduling variables: $\alpha \in [0, 20]$ deg, $V \in [160, 280]$ m/s, and $h \in [1, 14]$ km. For brevity, only a few flight conditions are shown among the overall ones analyzed in the process. The first parameter to be investigated is $\tilde{\rho}_1$. The results in Fig. 2(a) show how the value of the function has a negligible impact on the system dynamics. Coherently, the curves in Fig. 2(b), related to the complete entry of the state matrix, A_{12}, confirm the accuracy of the following approximation: $\tilde{\rho}_1 \approx 0 \mid A_{12}(\tilde{\rho}) = (1+\tilde{\rho}_1) \approx 1$. The number of scheduling functions, therefore, decreases to $n_{\tilde{\rho}} = 5$.

As observed in Eq. (11), the functions $\tilde{\rho}_2$, $\tilde{\rho}_5$, and $\tilde{\rho}_6$ have a common affine dependence on the dynamic pressure value, $\bar{q}$. In particular, the formulation of $\bar{q}$ itself includes the variations of two of the original scheduling variables: V and h. Thus, as a second form of system simplification, the three scheduling functions can be approximated uniquely as a function of the dynamic pressure. All the remaining parameters affecting $\tilde{\rho}_2$, $\tilde{\rho}_5$, and $\tilde{\rho}_6$ are frozen to a nominal average value in their range of variations, leading to:

$$\tilde{\rho}_2 := \frac{\bar{q}SC_{Z_{\delta_1}}\cos\alpha}{mV} \approx \frac{\bar{q}S\tilde{C}_{Z_{\delta_1}}}{m\tilde{V}}; \qquad \tilde{\rho}_5 := \frac{\bar{q}Sd^2C_{m_D}}{2I_{yy}V} \approx \frac{\bar{q}Sd^2\tilde{C}_{m_D}}{2I_{yy}\tilde{V}}; \qquad \tilde{\rho}_6 := \frac{\bar{q}SdC_{m_{\delta_1}}}{I_{yy}} \approx \frac{\bar{q}Sd\tilde{C}_{m_{\delta_1}}}{I_{yy}}.$$

In particular, the aerodynamic coefficients are functions of the Mach value, hence of V and h, but their variations are very limited. Similarly, the impact of the angle-of-attack variation on $\tilde{\rho}_2$ can be considered negligible for the present analysis. The accuracy of these approximations is verified in Fig. 3, where the variation of each of the three functions with respect to the original scheduling variables (α, V, h), is compared to the variations of their corresponding approximations. Thus, Figs. 3(a)-(c)-(e) provide the curve comparisons for $\tilde{\rho}_2$, $\tilde{\rho}_5$, and $\tilde{\rho}_6$, respectively, at different flight conditions. Additionally, Figs. 3(b)-(d)-(f) present the corresponding approximation errors, evaluated as the difference
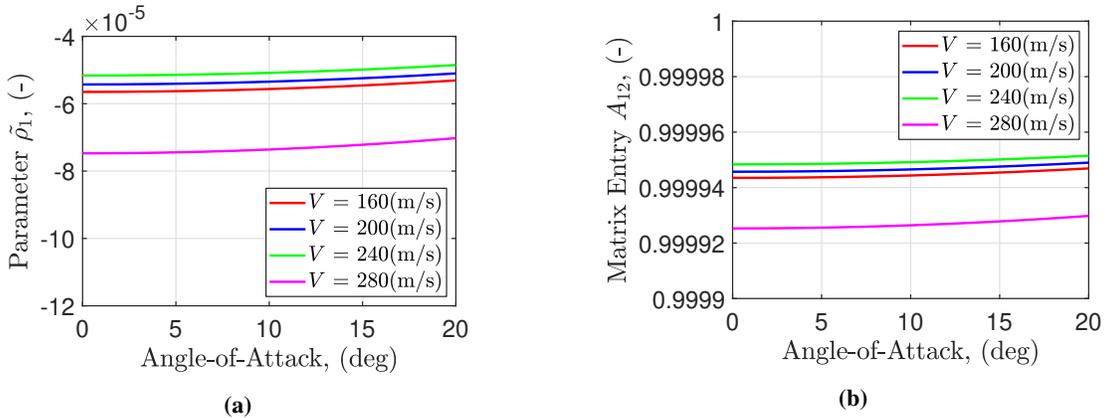

(a)

(b)

Fig. 2 **Approximation analysis: (a) $\tilde{\rho}_1$ variation at $h = 10$ km; (b) corresponding full matrix entry variation, A_{12}, at $h = 10$km.**

6

between the original and the approximated functions, and normalized by the mean values of the original curves. The results related to $\tilde{\rho}_2$ show a general maximum of 30% of error at the more extreme conditions of the investigated flight envelope, with a corresponding range of Normalized Root Mean Square Error (NRMSE) of [0.06, 0.28]. Similarly, the error evaluated for $\tilde{\rho}_5$ has an average value $\leq$ 10%, with a peak of 23%, and an NRMSE $\in$ [0.03, 0.22]. However, the most accurate approximation is observed in $\tilde{\rho}_6$, characterized by a peak $\leq$ 10% on a more general 2% of error, with an NRMSE $\in$ [0.001, 0.06]. Based on these results we can reduce the dimension of the new scheduling vector, $n_{\tilde{\rho}}$, by representing the variation of three scheduling functions in terms of the dynamic pressure variation, assumed to be the only parameter with a relevant impact on the functions.

The same analysis is proposed for the remaining functions, $\tilde{\rho}_3$ and $\tilde{\rho}_4$. However, the curves in Figs. 4(a)-(b) reveal the highly nonlinear behavior characterizing the derivatives of the equilibrium functions, especially for $\delta_{q,\text{eq}}(\rho)$.
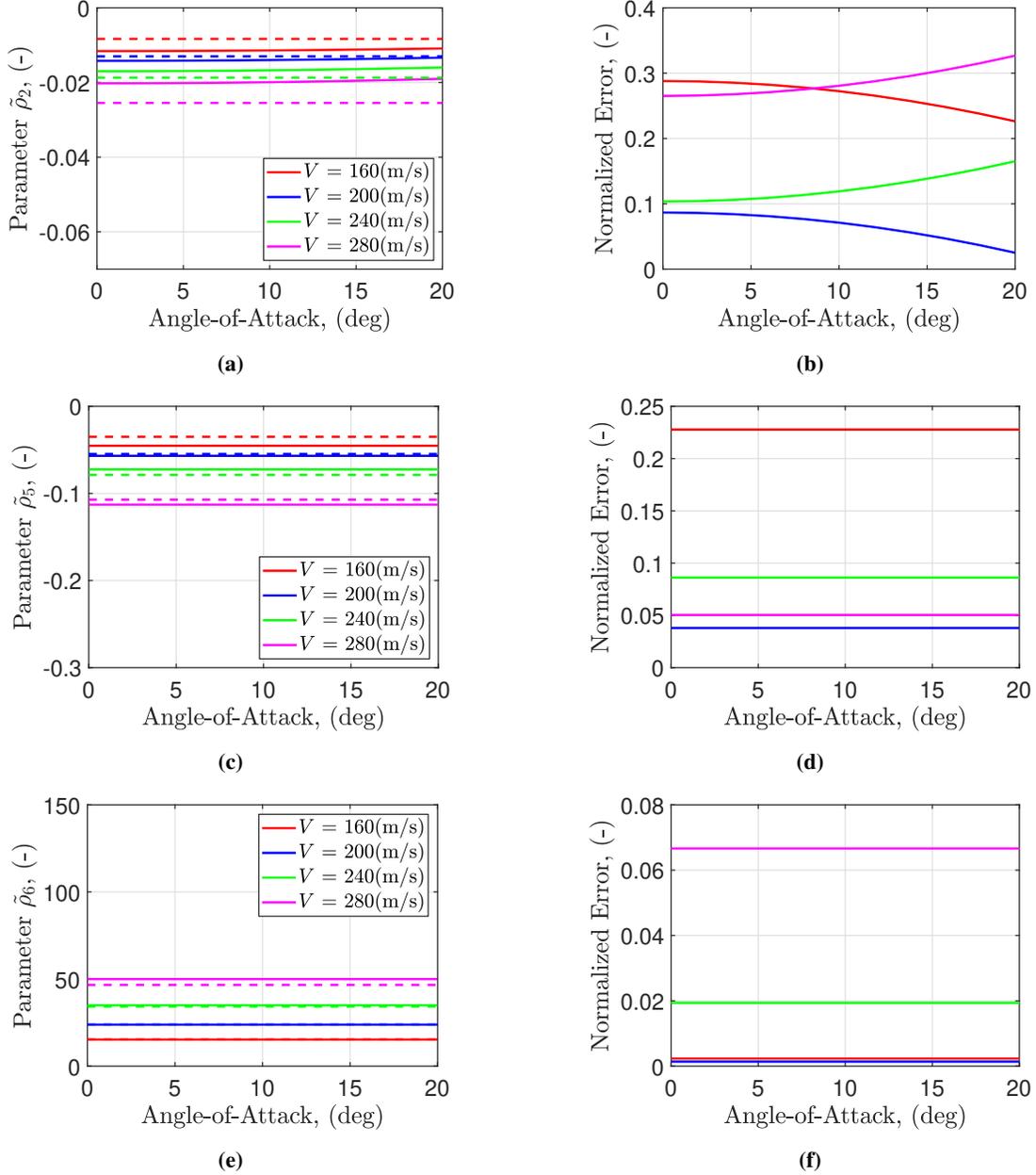

Fig. 3 Approximation analysis: (a)-(c)-(e) original (solid) and approximated (dashed) curve comparisons for $\tilde{\rho}_2$, $\tilde{\rho}_5$, and $\tilde{\rho}_6$, respectively; (b)-(d)-(f) corresponding normalized errors.
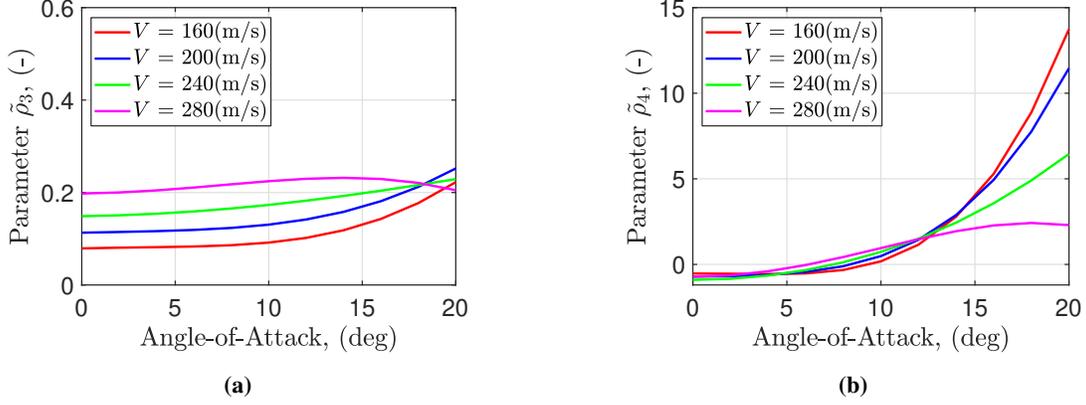
Fig. 4 Approximation analysis: (a) $\tilde{\rho}_3$ variation at $h = 10$ km; (b) $\tilde{\rho}_4$ variation at $h = 10$ km.

Additionally, their complex symbolic expressions prevent their expression as a linear function of the dynamic pressure, as previously done, as well as of the original set of scheduling variables. As a consequence, they are both directly included in $\tilde{\rho}$, as new scheduling functions.

The results can be summarized through the definition of the new scheduling vector $\hat{\rho} = [\hat{\rho}_1, \hat{\rho}_2, \hat{\rho}_3]$, with:

$$\hat{\rho}_1 := \bar{q}; \qquad \hat{\rho}_2 := \frac{\partial q_{\text{eq}}}{\partial \alpha}; \qquad \hat{\rho}_3 := \frac{\partial \delta_{q,\text{eq}}}{\partial \alpha}, \tag{13}$$

and the state matrix in Eq. (12) can be finally reformulated in a parameter affine form as:

$$\bar{A}(\hat{\rho}) = \begin{bmatrix} 0 & 1 & \bar{A}_{13}(\hat{\rho}_1) \\ 0 & \bar{A}_{22}(\hat{\rho}_1) - \hat{\rho}_2 & \bar{A}_{23}(\hat{\rho}_1) \\ 0 & -\hat{\rho}_3 & -\hat{\rho}_3 \bar{A}_{13}(\hat{\rho}_1) \end{bmatrix}, \tag{14}$$

where $\bar{A}_{13}$, $\bar{A}_{22}$, and $\bar{A}_{33}$ are the discussed approximated form of $\tilde{\rho}_2$, $\tilde{\rho}_5$, and $\tilde{\rho}_6$, respectively.

In order to assess the accuracy of the overall procedure, and to verify the impact of the new uncertainties on the dynamics of the system, a comparison between the pole-zero maps of the original (Full) and the approximated (Apprx.) models is proposed in Figs. 5. In particular, the two maps represent the poles/zeros of the systems at different flight conditions: Fig. 5(a) corresponds to an unstable $\alpha = 4$ deg and to increasing values of V and h; while Fig. 5(b) provides the same results assuming a stable $\alpha = 12$ deg. In both cases, it is possible to observe a slight difference between the original and the approximated poles at some flight conditions, especially for higher values of V and h. However, the effects of the approximations do not seem to generate relevant modifications in the system dynamics. These new forms of uncertainties will be taken into account at the control design stage, which is discussed in the next session.
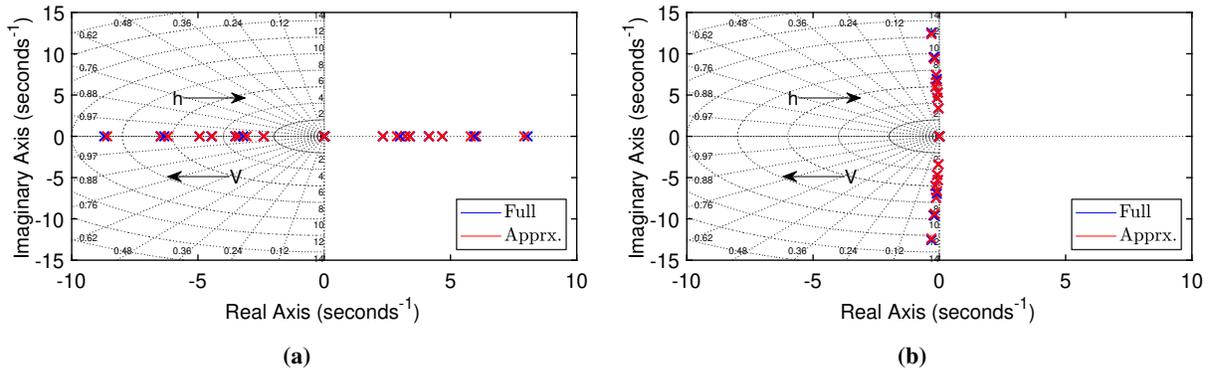

Fig. 5 Pole-zero maps comparison: (a) unstable condition $\alpha = 4$ deg; (b) stable condition $\alpha = 12$ deg.

8

C. Polytope Dimension Analysis

The final step of the approximation procedure consists of the analysis of the convex polytope defined by the new set of scheduling functions, $\hat{\rho} = [\hat{\rho}_1(V, h), \hat{\rho}_2(\alpha, V, h), \hat{\rho}_3(\alpha, V, h)]$. Indeed, it is necessary to properly map the original variation ranges $\alpha \in [0, 20]$ deg, $V \in [160, 280]$ m/s, and $h \in [1, 14]$ km, into the corresponding new ones to redefine the vertices of the polytope. A systematic procedure is developed to estimate the maximum/minimum values of each scheduling function across the entire set of flight conditions described by α, V, and h. A part of the results of the analysis is shown in Figs. 6(a)-(b)-(c), where the relations between the scheduling functions allow identifying the actual area of the fight envelope covered by the function variations. The estimated ranges of variation that define the new polytope correspond to $\hat{\rho}_1 \in [0.2, 4.4] \cdot 10^4$, $\hat{\rho}_2 \in [0.03, 0.62]$, and $\hat{\rho}_3 \in [-1, 3]$.

As a relevant remark, the minimum values for each scheduling function occur at the same flight point ($\alpha = 0$ deg, $V = 160$ m/s, $h = 14$ km). On the other side, the maximum values of $\hat{\rho}_1$ and $\hat{\rho}_2$ are obtained at the same conditions ($\alpha = 20$ deg, $V = 280$ m/s, $h = 1$ km), while $\hat{\rho}_3$ presents a peak value at ($\alpha = 20$ deg, $V = 230$ m/s, $h = 7825$ km). Despite this last slight difference, the results show a reasonable consistency between the original and the new polytope vertices, which can reduce the conservatism that might affect the later control design optimization. However, the polytope dimensions can be further optimized, since the selected variation ranges do not account for the physical relations between the scheduling variable trajectories. As a consequence, several areas of the polytope described by ($\hat{\rho}_1$, $\hat{\rho}_2$, $\hat{\rho}_3$), may correspond to inconsistent flight conditions in (α, V, h), increasing the conservatism of the optimization.

In order to adjust the dimension of the polytope, a set of ad-hoc designed guidance trajectories is employed as a reference for the estimation of the variables' physical relations. In particular, Fig. 6(d) presents the relation between V and h, which are affecting all the new scheduling functions. The curve reveals relevant inconsistency for flight conditions corresponding to high values of V combined with low values of h, as well as for low values of V in combination with high values of h. Looking at the Fig. 6(a), these conditions occur especially for $\hat{\rho}_1 \geq 2 \cdot 10^4$ & $\hat{\rho}_2 \geq 0.35$ and for $\hat{\rho}_1 \leq 0.5 \cdot 10^4$ & $\hat{\rho}_2 \leq 0.05$, respectively. Similarly, from Fig. 6(b), inconsistencies arise when $\hat{\rho}_3 \geq 2$ and for $\hat{\rho}_3 \leq -0.8$. Thus, the final optimized scheduling functions ranges employed in the polytope definition can be adjusted as $\hat{\rho}_1 \in [0.5, 2] \cdot 10^4$, $\hat{\rho}_2 \in [0.05, 0.35]$, and $\hat{\rho}_3 \in [-0.8, 2]$.
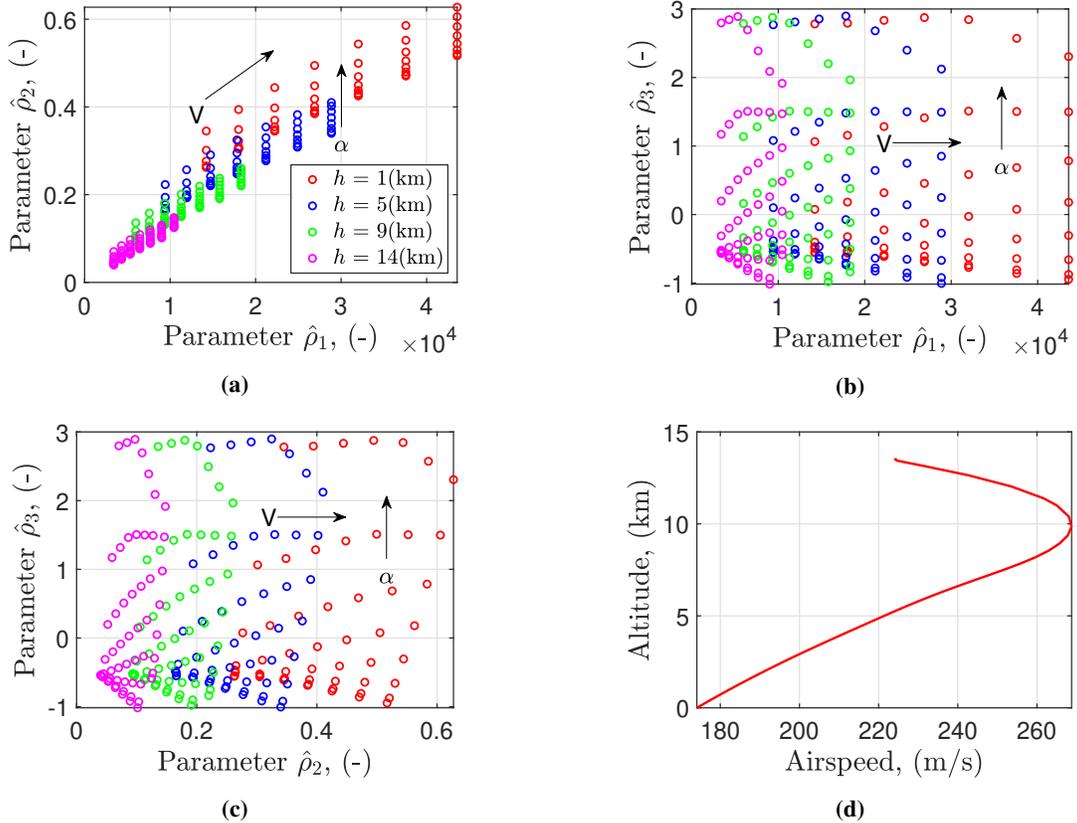

Fig. 6 **Scheduling parameter relations: (a) $\hat{\rho}_2 - \hat{\rho}_1$; (b) $\hat{\rho}_3 - \hat{\rho}_1$; (c) $\hat{\rho}_3 - \hat{\rho}_2$; (d) altitude-airspeed.**

IV. Polytopic Controller Design

In this section, the controller design methods and objectives are presented. The overall generalized plant architecture is first introduced, followed by the formulation of the LPV H_∞ controller optimization problem. The controller synthesis addresses the full flight envelope represented by the variation of the scheduling variables $\alpha \in [0, 20]$ deg, $V \in [160, 280]$ m/s, and $h \in [1, 14]$ km. The polytope is defined through the corresponding ranges of variation of the new set of scheduling functions $(\hat{\rho}_1, \hat{\rho}_2, \hat{\rho}_3)$, obtained in Section III as a result of the approximation process.

The frequency performances of the LPV H_∞ polytopic controller are compared with a state feedback modal design, based on the pole placement approach, which imposes the same dynamics at each of the flight conditions represented by the vertices of the polytope. The comparison emphasizes the benefits of the LPV approach by directly shaping the frequency properties of the closed-loop system, guaranteeing stability and performance at all flight conditions belonging to the polytope. Differently, a gain-scheduled controller obtained from the interpolation of the set of local LTI modal controllers would ensure no a priori stability properties for any intermediate flight conditions away from the vertices of the polytope.

A. Generalized Plant Architecture

The general architecture employed for LPV H_∞ controller design is presented in Fig. 7(a). A second-order model is included in the definition of the generalized plant to account for the actuator dynamics, together with the approximated *Augmented* quasi-LPV model described in Eqs. (13)-(14). A set of first-order weighting functions, W_e, and W_u, imposes the desired closed-loop performances by targeting the tracking error, $e = r - \alpha$, and the control deflection input, $\delta_{q,\mathrm{cmd}}$, respectively. The reference signal, r, consists of an angle-of-attack trajectory defined through a *Lift-to-Drag* ratio optimization law [30, 31]. The weighting functions are selected in a way to be coherent with the dynamics imposed during the pole placement design, to facilitate the later comparison between the two different approaches.

In particular, the shape of W_e is defined in order to ensure a reliable tracking capability of the reference signal, while the roll-off frequency of W_u is selected in accordance with the characteristic bandwidth of the actuator model. Additionally, a constant weight, $W_d = 0.1$, is applied to the input disturbance signal, d, aiming to improve the disturbance rejection properties of the controller. As a relevant remark, the weighting functions are independent of the scheduling functions, meaning that during the polytopic design the same performances are imposed at each vertex condition of the polytope, leading to possible conservativeness in the synthesis results.

The control scheme in Fig. 7(a) is then generalized as in Fig. 7(b), where the LPV plant, $P(\hat{\rho})$, includes the dynamics of the actuator, the projectile quasi-LPV polytopic model, and the weighting functions. Thus, the overall generalized state vector is defined as $x_P = [x, x_{\mathrm{act}}, x_{W_e}, x_{W_u}]^T \in \mathbb{R}^7$, with $x = [\alpha, q_{\mathrm{dev}}, \delta_{q,\mathrm{dev}}]^T \in \mathbb{R}^3$. The generalized exogenous input vector, $\omega = [r, d]^T \in \mathbb{R}^2$, accounts for the reference guidance signal and the input disturbance, while the control input, $u \in \mathbb{R}$, corresponds to the commanded virtual pitch deflection rate imposed to the canards, $\dot{\delta}_{q,\mathrm{cmd}}$. Finally, the generalized controlled output vector, $z = [z_1, z_2]^T \in \mathbb{R}^2$, includes the control optimization objectives, while the set of available measurements, $y = [e, q_{\mathrm{dev}}, \delta_{q,\mathrm{dev}}]^T \in \mathbb{R}^3$, is employed as input to the controller.

In the LPV polytopic control design, the generalized plant is evaluated at each flight condition corresponding to a vertex of the polytope by substituting the corresponding values of the scheduling functions. The resulting LTI realizations are employed in the formulation of the set of LMIs that defines the controller synthesis optimization.
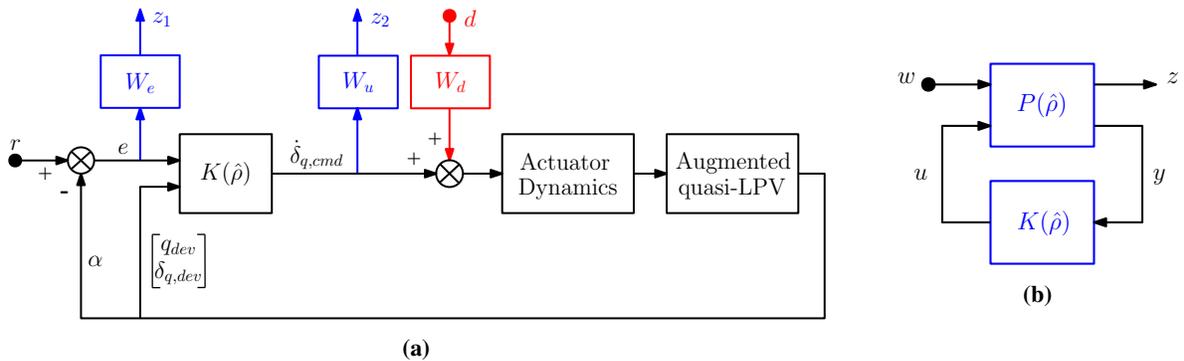

Fig. 7   Design scheme: (a) detailed architecture; (b) generalized plant.

B. Controller Synthesis Comparison

In the standard H_∞ robust control framework, the design aims to minimize the closed-loop induced L_2-norm, of the generalized plant previously defined, such that:

$$\|z\|_2 \le \gamma_\infty \|w\|_2; \qquad \gamma_\infty > 0 \tag{15}$$

The index, γ_∞, expresses how closely the frequency properties of the obtained closed-loop system match the desired performances, imposed by the weighting functions, W_e, W_u, and W_d, in the loop-shaping process.

In the specific case of the LPV polytopic design, the controller synthesis is formulated as the solution of a convex optimization problem, defined by the imposition of the same closed-loop performances at each realization of the LPV system. Thus, the optimization consists of a set of Linear Matrix Inequalities (LMIs) computed at each vertex of the polytope and solved offline with a constant Lyapunov function that guarantees the same stability and performance for each flight condition belonging to the polytope [29]. The solution corresponds to a set of LTI controllers, K_i, one for each of the vertices. The general polytopic controller, $K(\hat\rho)$, for any combinations of the scheduling functions vector, is obtained through the convex interpolation of the set of LTI controllers:

$$K(\hat\rho) = \sum_{i=1}^{2^{n_{\hat\rho}}} \mu_i(\hat\rho) K_i \tag{16}$$

As previously mentioned, the performances of the full LPV polytopic design are compared to an LTI state feedback design, based on the pole placement technique, where a controller is computed at each vertex condition of the selected polytope. Coherently to the LPV H_∞ design, the same dynamics are imposed at each vertex also in the case of the modal controllers.
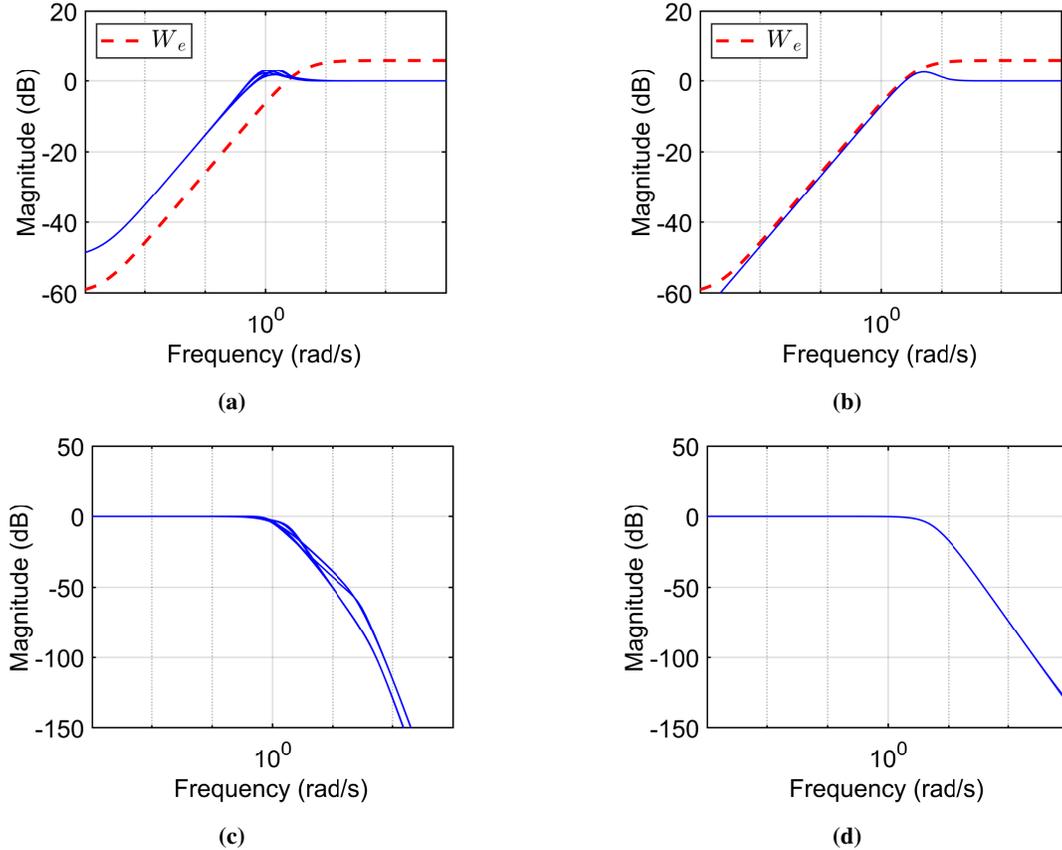

Fig. 8 Design results comparison: Sensitivity and Complementary Sensitivity functions related to (a)-(c) polytopic approach; (b)-(d) pole placement approach.

The design results obtained through the LTI pole placement approach and the LPV H_∞ technique, are compared in the frequency domain in Fig. 8 and Fig. 9. As a first observation, Figs. 8(a)-(b) show how the modal control design improves the transient dynamics properties of the system, which is slightly more responsive than in the polytopic case. Indeed, the tracking capability benefits from the faster dynamics imposed by targeting individually the flight conditions at each vertex of the polytope, while the LMIs optimization has to satisfy simultaneously the requirements at all the conditions. Therefore, the polytopic design is generally affected by a considerably higher level of conservativeness, which can deteriorate the performance of the controller. However, the high-frequency noise attenuation provided by the polytopic controller is more reliable than the capabilities obtained with the modal design, as shown in Figs. 8(c)-(d).

The main advantages provided by the LPV H_∞ polytopic synthesis are expressed in terms of the Plant Sensitivity and the Controller Sensitivity, presented in Fig. 9. Indeed, the polytopic controller is characterized by relevant low-frequency disturbance rejection properties, as in Fig. 9(a), observed homogeneously at each of the flight conditions described by the vertices of the polytope. Contrarily, the pole placement design in Fig. 9(b) succeeds in guaranteeing decent performances only at certain conditions, leaving the system generally affected by any sources of input disturbances. This represents an important aspect to be considered since the nonlinear pitch channel dynamics of the projectile have been subjected to several approximations, at first during the quasi-LPV transformation process, and later in the affine reformulation that generated the final polytopic model.

Concerning the performances imposed on the control effort by the weighting function, W_u, the polytopic controller respects perfectly the limitations at all the flight conditions, both in terms of the operating bandwidth and in terms of the low-frequency steady-state amplitude, as shown in Fig. 9(c). The results related to the pole placement design in Fig. 9(d), reveals that at higher frequencies the controller requires an excessive authority to stabilize the system than the one provided by the actuator dynamics. As a consequence, none of the LTI modal controllers at the polytope vertices would be implementable in practice, since they would generate immediate saturation of the canards.
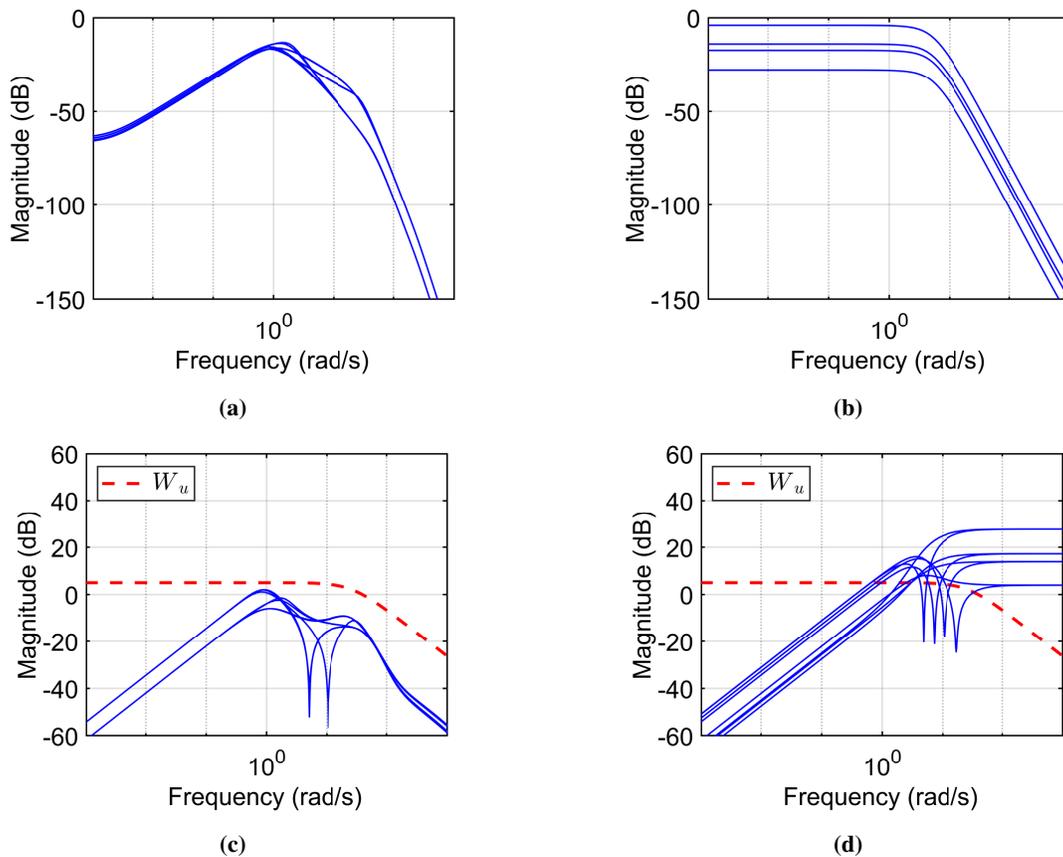

Fig. 9   Design results comparison: Plant Sensitivity and Controller Sensitivity functions related to (a)-(c) polytopic approach; (b)-(d) pole placement approach.

V. Trajectory Tracking Simulation

In this section, the LPV polytopic controller is tested in a trajectory tracking simulation scenario. The LTI gain-scheduled modal controller discussed in the previous section is not implemented, due to the unfeasible results observed in the frequency domain. The polytopic controller is applied directly on the full nonlinear pitch channel dynamics model of Eqs. (1)-(3), in order to test its capability to handle all the possible uncertainties introduced by the modeling and approximation process.

The simulation consists of a trajectory tracking scenario, where the reference signal corresponds to a realistic angle-of-attack trajectory, α_{ref}. The signal was previously obtained by testing a range-extending guidance law in a gliding phase flight scenario, defined through a *Lift-to-Drag* ratio optimization. The guidance simulations were applied on a planar point-mass model of the projectile. Since the pitch channel model in Eqs. (1)-(3) does not account for the dynamics of the airspeed and the altitude of the projectile, two reference signals are imposed in accordance with the results obtained with the guidance simulator, as presented in Figs. 10(a)-(b), respectively.

The simulation aims to cover most of the range of variation of each scheduling variable to assess the performances of the controller and to verify which areas of the polytope are actually interested by trajectory.
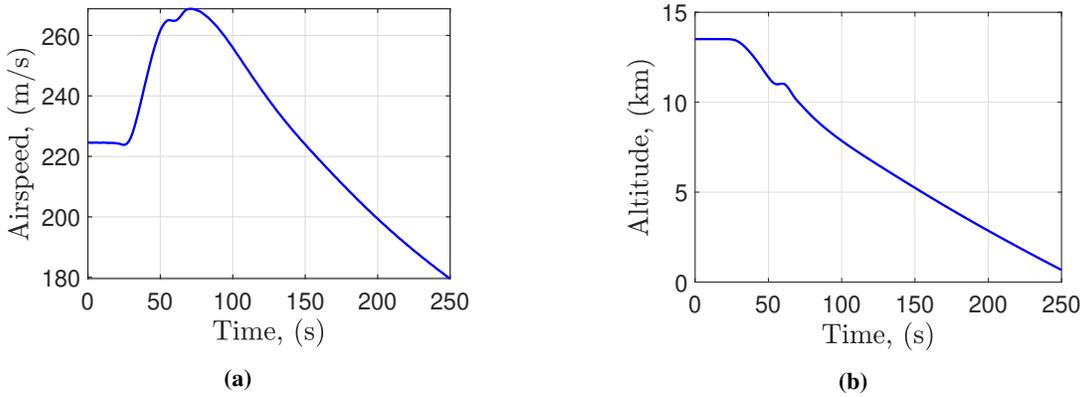

(a)

(b)

Fig. 10   Guidance trajectories: (a) reference airspeed; (b) reference altitude.

A. Simulator Architecture

The scheme in Fig. 11 presents the actual implementation of the LPV controller on the nonlinear projectile dynamics. In particular, an integrator is interposed between the output of the controller and the input of the actuator model. Indeed, the quasi-LPV model obtained through the State Transformation technique in Eqs. (7)-(8), was augmented with an integrator at the input to cancel the internal feedback loop affecting the stability of the system. Thus, the output of the controller is integrated before being processed by the nonlinear model to ensure consistency between the two models.

Similarly, the output of the nonlinear system, (α, q, δ_q), is deviated in post-processing in order to comply with the formulation of the transformed state vector in Eq. (6), where q_{dev} and $\delta_{q,\text{dev}}$ represent the non-scheduling off-equilibrium states of the quasi-LPV model. Therefore, the *Output Deviation* block in Fig. 11 evaluates the equilibrium functions, q_{eq}, and $\delta_{q,\text{eq}}$, at each flight condition to properly correct the output of the nonlinear system. These implementation solutions can result in additional sources of model uncertainties that may affect the robustness properties of the controller.
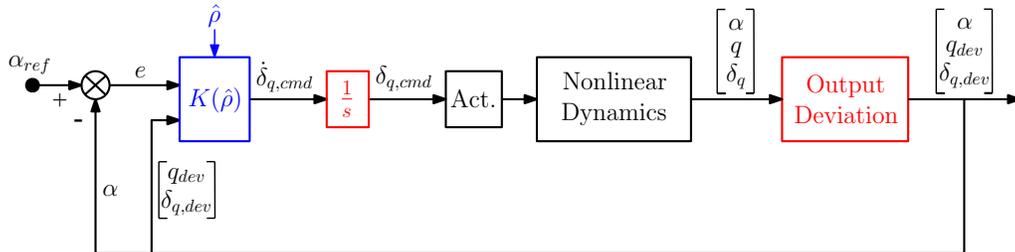

Fig. 11   Trajectory tracking simulation scheme.

13

B. Simulation Results

The controller tracking performances on the nonlinear dynamic model are shown in Fig. 12(a). A sudden oscillation is observed at the initialization of the controller, which depends on the mismatch between the nonlinear and the quasi-LPV model formulations. Indeed, the quasi-LPV model was derived on base of the aerodynamics approximations (nonlinear *Simplified* model), discussed in Section II. Thus, a small difference affects the initial conditions characterizing the controller and the ones characterizing the nonlinear system.

However, the controller succeeds in rapidly compensating the oscillation and converging to the reference signal, ensuring reliable tracking performances along the entire angle-of-attack trajectory, which covers most of the flight envelope described by the polytopic design. A slight steady state tracking error $< 2\%$ is observed after the initial transient when the guidance signal stabilizes around a fixed value. The mismatch derives from the uncertainties introduced
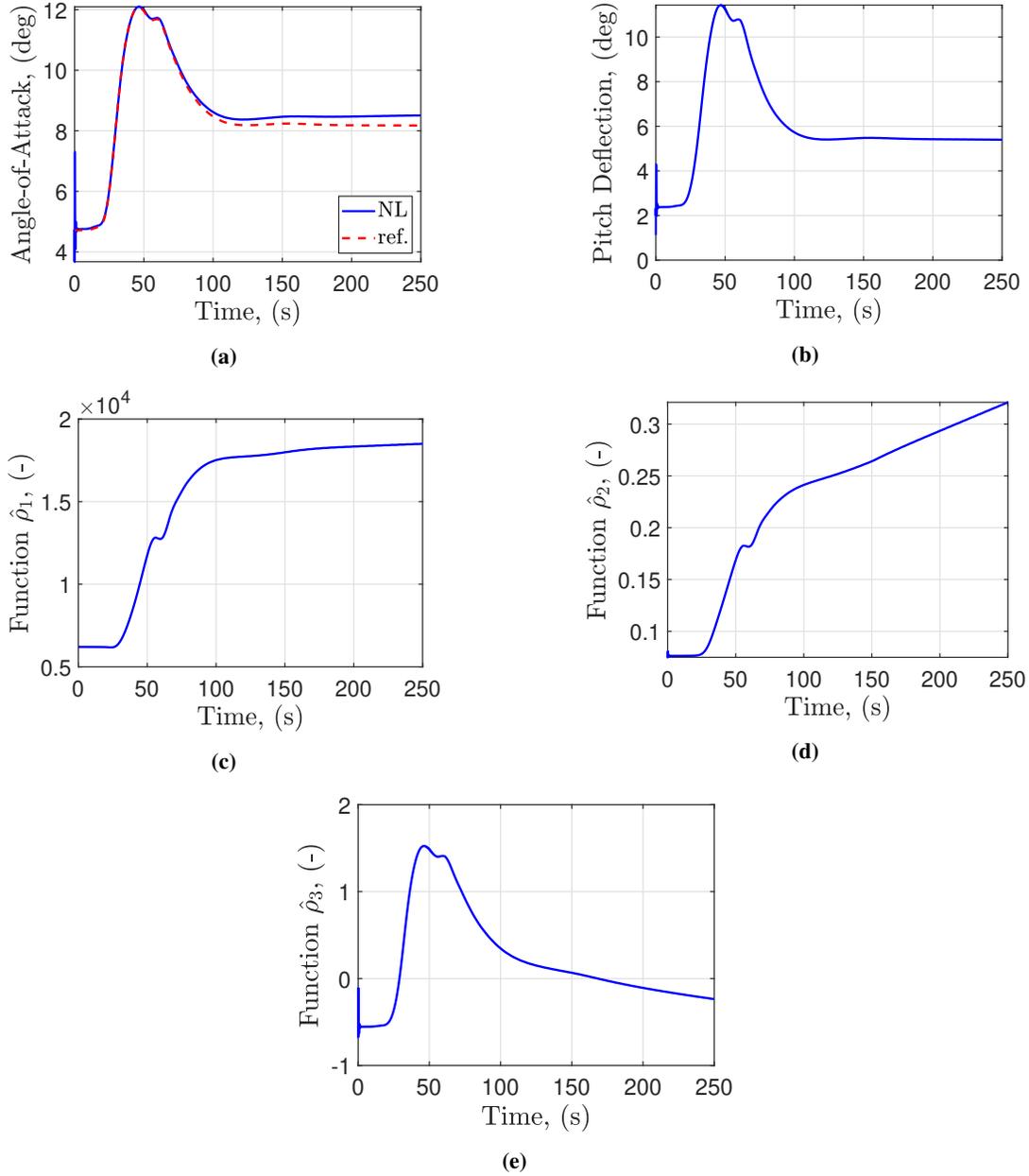

Fig. 12   Simulation results: (a) angle-of-attack trajectories; (b) pitch deflection input; (c) scheduling function, $\hat{\rho}_1$; (d) scheduling function, $\hat{\rho}_2$; (e) scheduling function, $\hat{\rho}_3$.

during the modeling approximation process, as well as from the responsiveness of the system that is characterized by a limited control authority. Nevertheless, the disturbance rejection properties imposed at the design stage provide the controller with the capability to stabilize the projectile dynamics and to minimize the tracking error to a reasonable level, across the entire flight envelope.

Another relevant observation is related to the required control effort. Indeed, Fig. 12(b) shows how the input signal corresponding to the total pitch deflection angle, α_{can}, is maintained at a relatively low amplitude during the trajectory, far below the saturation limits. The total pitch deflection is the overall deflection angle perceived by the canards, expressed as the linear superposition between the local pitch deflection, δ_q, commanded by the controller, and the angle-of-attack characterizing the trajectory of the projectile, as $\alpha_{can} = \alpha + \delta_q$.

As a final remark, Figs. 12(c)-(d)-(e) present the simulation trajectory related to the three scheduling functions: $\hat{\rho}_1$, $\hat{\rho}_2$, and $\hat{\rho}_3$, respectively. It is interesting to notice the quasi-linear relation characterizing the functions $\hat{\rho}_1$ and $\hat{\rho}_2$, already observed during the polytope analysis in Section III. On the other side, the scheduling function $\hat{\rho}_3$ shows an evident dependence on the variation of the angle-of-attack, since the trajectories have very similar shapes. This information can be used for a further process of optimization of the polytope dimension. However, the boundary values of each scheduling function are perfectly consistent with the variation ranges selected during the polytope analysis.

These results confirm the quality of the modeling and approximation process performed to convert the nonlinear pitch channel dynamics of the projectile into a quasi-LPV polytopic model, as well as the advantages of the polytopic controller design. Indeed, the resolution of the set of LMIs only at the vertices of the polytope reduces drastically the overall computational complexity, allowing the synthesis of a controller able to stabilize the system at any flight conditions belonging to the polytope. As a drawback, the polytopic approach tends to generate conservative results that can deteriorate the performance of the controller, as observed for the tracking capability. Thus, a proper analysis of the scheduling variable ranges is required to optimize the polytope shape and dimension.

VI. Conclusions and Future Work

In this article, the nonlinear pitch channel dynamics of a Long Range Guided Projectile are presented and converted to a reliable quasi-LPV model using the State Transformation method. The quasi-LPV model is later reformulated in order to comply with the polytopic requirements of an affine model-parameter relation, through a process that maps the original set of scheduling variables into a new set of scheduling functions. The resulting quasi-LPV polytopic model is employed for the design of a pitch controller, with the intention to track a given angle-of-attack reference signal. Two different approaches are investigated: a modal state feedback design, based on the pole placement approach, and a H_∞ LPV polytopic design. The latter approach is expected to provide the same guaranteed performance for all the flight conditions belonging to the analyzed flight envelope.

The controller synthesis is performed on the flight envelope defined by the variation of the scheduling functions of the LPV polytopic model. The investigated envelope is modeled as a convex subspace (polytope), whose vertices correspond to the combination of the boundary values of each scheduling function. Both the LPV polytopic design and the LTI modal approach are employed for controller development. The design results in the frequency domain show how, despite the less responsive tracking performance, the polytopic controller ensures relevant disturbance rejections and reasonable control requirements properties at all the investigated flight conditions. Differently, the modal controller guarantees higher tracking capability, but poor disturbance rejection, and requires an unfeasible control effort with respect to the limitations imposed by the actuator dynamics. Finally, a gliding phase simulation scenario, involving the full variation range of the scheduling functions, confirms the capability of the LPV polytopic controller to successfully stabilize the projectile dynamics and to track a reference angle-of-attack guidance trajectory.

In terms of future work, the performances of the polytopic controller will be improved by optimizing the size of the investigated polytope. Indeed, the scheduling function trajectories observed during simulation tests appear to belong to a limited subset of the flight envelope described by the vertices of the polytope, suggesting that the controller synthesis optimization is probably still accounting for inconsistent flight conditions. A more trajectory-based polytope definition is expected to enhance the tracking capability and optimize the required control effort, by reducing the level of conservativeness affecting the controller synthesis. The range-extending guidance law will be further developed through the inclusion of the projectile roll-yaw channels dynamics to additionally provide a reference roll-angle trajectory for the implementation of a full Bank-to-Turn flight strategy.

References

[1] Shamma, J. S., and Cloutier, J. R., "Gain-scheduled missile autopilot design using linear parameter varying transformations," *Journal of guidance, Control, and dynamics*, Vol. 16, No. 2, 1993, pp. 256–263. https://doi.org/10.2514/3.20997.

[2] Carter, L. H., and Shamma, J. S., "Gain-scheduled bank-to-turn autopilot design using linear parameter varying transformations," *Journal of guidance, control, and dynamics*, Vol. 19, No. 5, 1996, pp. 1056–1063. https://doi.org/10.2514/3.21745.

[3] Prempain, E., Postlethwaite, I., and Vorley, D., "A gain scheduled autopilot design for a bank-to-turn missile," *Proceedings of the 2001 European Control Conference (ECC)*, IEEE, Porto, Portugal, 2001, pp. 2052–2057. https://doi.org/10.23919/ECC.2001.7076224.

[4] Theodoulis, S., and Proff, M., "Robust Flight Control Tuning for Highly Agile Missiles," *AIAA Scitech 2021 Forum*, Virtual event, 2021, p. 1568. https://doi.org/https://doi.org/10.2514/6.2021-1568.

[5] Tan, W., Packard, A. K., and Balas, G. J., "Quasi-LPV modeling and LPV control of a generic missile," *Proceedings of the 2000 American Control Conference. ACC (IEEE Cat. No. 00CH36334)*, Vol. 5, IEEE, Chicago, IL, US, 2000, pp. 3692–3696. https://doi.org/10.1109/ACC.2000.879259.

[6] Balas, G. J., Fialho, I., Packard, A., Renfrow, J., and Mullaney, C., "On the design of LPV controllers for the F-14 aircraft lateral-directional axis during powered approach," *Proceedings of the 1997 American Control Conference (Cat. No. 97CH36041)*, Vol. 1, IEEE, Albuquerque, NM, US, 1997, pp. 123–127. https://doi.org/10.1109/ACC.1997.611768.

[7] Yue, T., Wang, L., and Ai, J., "Gain self-scheduled H_∞ control for morphing aircraft in the wing transition process based on an LPV model," *Chinese journal of aeronautics*, Vol. 26, No. 4, 2013, pp. 909–917. https://doi.org/10.1016/j.cja.2013.06.004.

[8] Hjartarson, A., Seiler, P., and Balas, G. J., "LPV analysis of a gain scheduled control for an aeroelastic aircraft," *2014 American Control Conference*, IEEE, Portland, OR, US, 2014, pp. 3778–3783. https://doi.org/10.1109/ACC.2014.6859301.

[9] Sève, F., Theodoulis, S., Wernert, P., Zasadzinski, M., and Boutayeb, M., "Pitch/yaw channels control design for a 155mm projectile with rotating canards, using a H_∞ loop-shaping design procedure," *AIAA Guidance, Navigation, and Control Conference*, National Harbor, MD, US, 2014, p. 1474. https://doi.org/10.2514/6.2014-1474.

[10] Theodoulis, S., Gassmann, V., Wernert, P., Dritsas, L., Kitsios, I., and Tzes, A., "Guidance and control design for a class of spin-stabilized fin-controlled projectiles," *Journal of Guidance, Control, and Dynamics*, Vol. 36, No. 2, 2013, pp. 517–531. https://doi.org/10.2514/1.56520.

[11] Theodoulis, S., Sève, F., and Wernert, P., "Robust gain-scheduled autopilot design for spin-stabilized projectiles with a course-correction fuze," *Aerospace Science and Technology*, Vol. 42, 2015, pp. 477–489. https://doi.org/10.1016/j.ast.2014.12.027.

[12] Strub, G., Theodoulis, S., Gassmann, V., Dobre, S., and Basset, M., "Gain-scheduled autopilot design and validation for an experimental guided projectile prototype," *Journal of Guidance, Control, and Dynamics*, Vol. 41, No. 2, 2018, pp. 461–475. https://doi.org/10.2514/1.G002916.

[13] Sève, F., and Theodoulis, S., "Design of an H_∞ Gain-Scheduled Guidance Scheme for a Guided Projectile," *Journal of Guidance, Control, and Dynamics*, Vol. 42, No. 11, 2019, pp. 2399–2417. https://doi.org/10.2514/1.G004317.

[14] Shamma, J. S., and Athans, M., "Gain scheduling: Potential hazards and possible remedies," *IEEE Control Systems Magazine*, Vol. 12, No. 3, 1992, pp. 101–107. https://doi.org/10.1109/37.165527.

[15] Leith, D. J., and Leithead, W. E., "Survey of gain-scheduling analysis and design," *International journal of control*, Vol. 73, No. 11, 2000, pp. 1001–1025. https://doi.org/10.1080/002071700411304.

[16] Marcos, A., and Balas, G. J., "Development of linear-parameter-varying models for aircraft," *Journal of Guidance, Control, and Dynamics*, Vol. 27, No. 2, 2004, pp. 218–228. https://doi.org/10.2514/1.9165.

[17] Balas, G. J., "Linear, parameter-varying control and its application to aerospace systems," *Proceedings of the ICAS congress*, Toronto, Canada, 2002.

[18] Poussot-Vassal, C., and Roos, C., "Generation of a reduced-order LPV/LFT model from a set of large-scale MIMO LTI flexible aircraft models," *Control Engineering Practice*, Vol. 20, No. 9, 2012, pp. 919–930. https://doi.org/10.1016/j.conengprac.2012.06.001.

[19] Wu, F., Packard, A., and Balas, G., "LPV control design for pitch-axis missile autopilots," *Proceedings of 1995 34th IEEE Conference on Decision and Control*, Vol. 1, IEEE, New Orleans, LA, US, 1995, pp. 188–193. https://doi.org/10.1109/CDC.1995.478672.

[20] Pfifer, H., and Hecker, S., "LPV controller synthesis for a generic missile model," *2010 IEEE International Conference on Control Applications*, IEEE, Yokohama, Japan, 2010, pp. 1838–1843. https://doi.org/10.1109/CCA.2010.5611127.

[21] Pfifer, H., and Hecker, S., "Generation of optimal linear parametric models for LFT-based robust stability analysis and control design," *IEEE Transactions on Control Systems Technology*, Vol. 19, No. 1, 2010, pp. 118–131. https://doi.org/10.1109/TCST.2010.2076329.

[22] Pellanda, P. C., Apkarian, P., and Tuan, H. D., "Missile autopilot design via a multi-channel LFT/LPV control method," *International Journal of Robust and Nonlinear Control: IFAC-Affiliated Journal*, Vol. 12, No. 1, 2002, pp. 1–20. https://doi.org/10.1002/rnc.612.

[23] Bryson, J., and Gruenwald, B. C., "Linear Parameter Varying Model Predictive Control of a High-Speed Projectile," *AIAA SCITECH 2022 Forum*, San Diego, CA, US, 2022, p. 1585. https://doi.org/10.2514/6.2022-1585.

[24] Fresconi, F., "Guidance and control of a projectile with reduced sensor and actuator requirements," *Journal of Guidance, Control, and Dynamics*, Vol. 34, No. 6, 2011, pp. 1757–1766. https://doi.org/10.2514/1.53584.

[25] Cooper, G., Fresconi, F., and Costello, M., "Flight stability of an asymmetric projectile with activating canards," *Journal of Spacecraft and Rockets*, Vol. 49, No. 1, 2012, pp. 130–135. https://doi.org/10.2514/1.A32022.

[26] Vasile, J. D., Bryson, J., Gruenwald, B. C., Fairfax, L., Strohm, L., and Fresconi, F., "A Multi-Disciplinary Approach to Design Long Range Guided Projectiles," *AIAA Scitech 2020 Forum*, Orlando, FL, US, 2020, p. 1993. https://doi.org/10.2514/6.2020-1993.

[27] Vinco, G. M., Theodoulis, S., and Sename, O., "Flight Dynamics Modeling and Simulator Design for a New Class of Long-Range Guided Projectiles," *CEAS EuroGNC Conference*, Berlin, Germany, 2022. URL https://hal.univ-grenoble-alpes.fr/hal-03654390.

[28] Vinco, G. M., Theodoulis, S., Sename, O., and Strub, G., "Quasi-LPV modeling of Guided Projectile Pitch Dynamics through State Transformation Technique," *5th IFAC Workshop on Linear Parameter Varying Systems (LPVS)*, Montreal, Canada, 2022. URL https://hal.univ-grenoble-alpes.fr/hal-03690075.

[29] Apkarian, P., Gahinet, P., and Becker, G., "Self-scheduled H_∞ control of linear parameter-varying systems: a design example," *Automatica*, Vol. 31, No. 9, 1995, pp. 1251–1261. https://doi.org/10.1016/0005-1098(95)00038-X.

[30] Phillips, C. A., "Guidance algorithm for range maximization and time-of-flight control of a guided projectile," *Journal of Guidance, Control, and Dynamics*, Vol. 31, No. 5, 2008, pp. 1447–1455. https://doi.org/10.2514/1.31327.

[31] Kelley, H. J., Cliff, E. M., and Lutze, F. H., "Boost–glide range-optimal guidance," *Optimal Control Applications and Methods*, Vol. 3, No. 3, 1982, pp. 293–298. https://doi.org/10.1002/oca.4660030307.